Transparent photodetectors with ultra-low dark current and high photoresponse for near-infrared detection

by Marvin Yonathan Hadiyanto

Submission date: 17-Apr-2023 07:16AM (UTC+0700)
Submission ID: 2066381668
File name: 9_OE_1-s2.0-S1566119921002913-main.pdf (4.37M)
Word count: 7334
Character count: 37087

Organic Electronics 99 (2021) 106356

Contents lists available at ScienceDirect

Organic Electronics

journal homepage: www.elsevier.com/locate/orgel

Transparent photodetectors with ultra-low dark current and high photoresponse for near-infrared detection

Marvin Yonathan Hadiyanto [a,b,1], Richie Estrada [a,c,1], Chih-Chien Lee [c], Sajal Biring [a,b], Abdul Khalik Akbar [a], Chien-Yi Li [c], Chun-Jen Shih [a], Ya-Ze Li [c], Shun-Wei Liu [a,b,*]

[a] Organic Electronics Research Center, Ming Chi University of Technology, New Taipei City 24301, Taiwan
[b] Department of Electronic Engineering, Ming Chi University of Technology, New Taipei City 24301, Taiwan
[c] Department of Electronic Engineering, National Taiwan University of Science and Technology, Taipei 10607, Taiwan

ARTICLE INFO

Keywords:
Transparent organic photodetectors
OPD
Photoresponse
Dark current density
Near-infrared detection

ABSTRACT

A remarkable progress in research works regarding flexibility and transparency of organic optoelectronic devices has been observed in the past decade compared to their inorganic counterparts. However, few studies have been devoted to the advancement of a transparent organic photodetector. In this study, we have used a wavelength-selective bulk-heterojunction of ClAlPc:C_{60} as active layer and Cu:Ag/WO_3 metal alloy as electrode to realize a see-through organic photodetector (OPD) with an average visible transmission of 76.92%. The optimized transparent OPDs show an average dark current density of 0.36 nA cm^{-2} and a rise/fall time of <5 μs under a bias voltage of −2 V, which could be potentially applied in a home security system based on invisible near-infrared detection.

1. Introduction

Organic photodetectors (OPDs) with low dark current density, large linear dynamic range (LDR), and high detectivity show a high potential to compete with the conventional inorganic photodetectors (PDs) [1,2]. OPDs possess few extraordinary characteristics that the inorganic PDs suffer from, such as large-area devices, mechanical flexibility, light-weight, and low-cost processes [2]. Moreover, features of OPDs such as transparency and tunability in wavelength detection find unique applications in image sensing, fluorescence detection, and colorimetry [3,4]. As per requirements, transparent OPDs should be combined with highly responsive photoactive material and highly transparent electrodes for successful practical applications [5,6].

Thin photoactive layer with a selective wavelength absorption ability is required to realize an effective transparent OPDs [7–9]. For example, semitransparent OPDs fabricated by Kim et al. implemented the bulk-heterojunction active layer of dicyanovinyl substituted terthiophene derivative (DCV3T) *N*,*N*-dimethylquinacr-idone (DMQA) with its bulk thickness as thin 110 nm [9]. Their devices suffered a low transparency of 26% in the blue region due to high absorption by the active material in the blue wavelength. To avoid absorption in the visible region, chloroaluminum phthalocyanine (ClAlPc) is a suitable candidate due to its absorption is in the near-infrared (NIR) region [10,11]. For instance, application of fullerene (C_{60}) material as an acceptor and ClAlPc as a donor for the bulk-heterojunction of ClAlPc:C_{60} as fabricated by Li et al. successfully demonstrated a transparent organic photovoltaic (OPV) with AVT up to 77.45%, while Verreet et al. achieved 3% cell efficiency with ClAlPc:C_{60} based OPVs by the aid of structural templating method [12,13]. Although the bulk-heterojunction of ClAlPc:C_{60} was applied in the OPVs, this kind of active layer is promising to be used in the structure of transparent OPDs, since OPDs can be built based on the structure of the OPV as demonstrated recently by Lee et al. [10]. As an alternative to the bulk-heterojunction, the bilayer structure of ClAlPc/C_{60} introduced by Wei et al. provided AVT of 72% [14]. Various blending layers from derivative of metallo-phthalocyanine (MPc) and fullerene (C_{60} or C_{70}), i.e., the sandwiched structure of ClAlPc/ClAlPc:C_{60}/C_{60} [15], horizontal bulk-heterojunction structure of CuPc:C_{60}/ClAlPc:C_{60} [16], bulk-heterojunction structure of ClAlPc:C_{70} [17], and bilayer structure from various types of MPc such as ClAlPc, boron(III) subphthalocyanine chloride (SubPc), and copper(II) phthalocyanine (CuPc) as the donor with C_{70} as the acceptor [18], were also further investigated for OPVs

* Corresponding author. Organic Electronics Research Center, Ming Chi University of Technology, New Taipei City 24301, Taiwan.
E-mail address: swliu@mail.mcut.edu.tw (S.-W. Liu).
[1] M. Y. Hadiyanto and R. Estrada are equally contributed to this work.

https://doi.org/10.1016/j.orgel.2021.106356
Received 17 July 2021; Received in revised form 15 September 2021; Accepted 15 September 2021
Available online 1 October 2021

applications. Moreover, ClAlPc also successfully demonstrated beyond the OPV or OPD applications, Shih et al. recently proposed the organic upconversion device (infrared to visible light upconversion) based on single photoactive material, ClAlPc [19]. Even though these studies were not conducted to develop transparent OPD, these materials have a low absorption in visible wavelengths that promising for the emerging transparent OPDs. Furthermore, the transparency and overall device transmittance also play a crucial role in transparent OPD performances. Mostly, the transparency level of a device depends on the transmittance of transparent electrodes. Many research groups have proposed several solutions for the transparent electrodes. Recently, a highly conducting poly(3,4-ethylenedioxythiophene)-polystyrene sulfonate is applied as a transparent electrode in the self-powered NIR OPDs with a large LDR of 154 dB [20]. Widely known transparent electrode of dielectric/metal/dielectric (DMD) multilayered structure, such as tungsten (VI) oxide (WO_3)/Ag/WO_3 or WAW, molybdenum(VI) oxide (MoO_3)/Ag/WO_3 or MAW, and bathocuproine (BCP)/Ag/MoO_3 offering the transmittance of >80%, 88%, and >75%, respectively [21–24]. The application of graded silver electrode was also reported by Liu et al. with a transmittance of ~75% [25]. Furthermore, other research works have successfully proposed various dielectric-metal electrodes, such as a dielectric-metal hybrid layer of fluorolithium (LiF):Al, nanostructured metal Ca:Ag/MoO_3, and thin metal alloy Cu:Ag/WO_3 with a transmittance of 70%, 95%, and >75%, respectively [12,26,27]. Among these methods, transparent electrode of Cu:Ag/WO_3 is highly promising with an affordable cost in the aspects of transparency, conductivity, and simplicity in the fabrication process simultaneously, especially for the device fabrication with a vacuum deposition process.

In this work, we have reported the transparent OPDs along with the reference OPDs as the performances indicator. The OPDs were fabricated by a vacuum deposition process with the bulk-heterojunction active layer of ClAlPc:C_{60} at the mixing ratio of 1:2, 1:4, and 1:6. To gain a high transparency, we followed a method proposed in the previous study by utilized the transparent electrode of thin metal Cu:Ag capped with WO_3 layer in the transparent OPDs, while opaque metal electrode of Ag layer was used in the reference OPDs. Optical and electrical characterizations such as dark current density, external quantum efficiency (EQE), specific detectivity (D*), LDR, -3dB limited frequency bandwidth (f_{-3dB}), transient photoresponse, ultraviolet–visible (UV–vis) spectroscopy, and impedance spectroscopy were investigated to examine the OPDs performances in an ambient environment. The optimized transparent OPDs showed an average dark current density of 0.36 nA cm^{-2}, AVT of 76.92%, and specific detectivity of 4.12 × 10^{12} Jones at applied bias of −2 V in the wavelength of 780 nm. On the other hand, the reference OPDs achieved an average dark current density of 4.13 nA cm^{-2} and a specific detectivity of 1.94 × 10^{12} Jones under the same applied bias and wavelength. These results demonstrate the transparent OPDs with a lower dark current density (higher detectivity) than the reference OPDs. For comparison, our transparent OPDs are comparable with the transparent self-powered NIR OPDs reported by Zhu et al. that perform a decent linear dynamic range of 154 dB and responsivity of 0.28 A W^{-1} [20]. On the other hand, our proposed transparent OPDs exhibit sub-nA cm^{-2} dark current density and AVT ~77%. Furthermore, both transparent OPDs achieved the detectivity at the order of 10^{12} Jones. In comparison with the other previous results, our transparent OPDs show a superior performances (see Fig. 1). [7,9,28–32].

2. Experiment

2.1. Materials and device fabrication

The materials such as *N*,*N*′-Bis(naphthalen-1-yl)-*N*,*N*′-bis(phenyl) benzidine (NPB), 4,7-diphenyl-1,10-phenanthroline (BPhen), ClAlPc, C_{60}, WO_3, Ag, and Cu were purchased from Merck KGaA (Sigma-Aldrich). ClAlPc had been sublimated two times under a vacuum

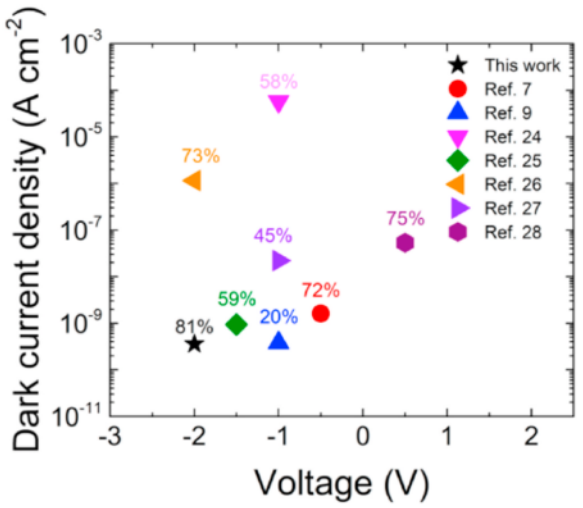

Fig. 1. Dark current density versus voltage plot of the state-of-the-art transparent OPDs. The number above the symbol points denotes the transmittance values of these devices measured at wavelength of 515 nm.

environment (2 × 10^{-5} torr) by a homemade purification system before the fabrication process. The thin layer of materials was deposited on the indium tin oxide (ITO)-coated glass substrate (Luminescence Technology Corp., 15 Ω sq^{-1}). The reference OPDs with the structure of ITO/NPB (25 nm)/ClAlPc:C_{60} (40 nm; 1:2)/BPhen (3 nm)/Ag (80 nm) and transparent OPDs with the structure of ITO/NPB (25 nm)/ClAlPc:C_{60} (40 nm; 1:x; with x = 2, 4, and 6)/BPhen (3 nm)/Cu:Ag (8 nm; 1:50)/WO_3 (40 nm) were fabricated by vacuum deposition process. The active area of OPDs is 0.04 cm^2. All thin films were deposited in a thermal evaporator under 3 × 10^{-6} torr with a deposition rate of 0.05–0.3 Å s^{-1} (2.5–3 Å s^{-1} for Ag). After the deposition process, the samples were encapsulated in a N_2 glove box (Oxygen <0.1 ppm and moisture <0.1 ppm) with bare glass and glued with UV-curable epoxy resin under UV light. All thin films were deposited on the bare glass.

2.2. Device characterization

Dark current density-voltage and spectral noise density measurements of OPDs were measured by Keithley 2636 with Labview measurement software. The measurements were carried out in dark conditions. EQE and responsivity spectrums were measured by QE-R Solar cell Spectral Response Measurement System of Enli Technology Co., Ltd. Taiwan, and monochromatic light chopped at 200 Hz calibrated by silicon and germanium photodetectors in the QE-R system. The EQE and responsivity of transparent OPDs were measured for both top side (metal electrode) and bottom side (ITO) illumination. LDR were measured by the homemade LDR measurement system, which consists of LED with wavelength 780 nm (Thorlabs, M780L3) used as the illumination source directed to the filter wheel (Thorlabs, FW102CNEB). The output from the filter wheel was used to illuminate the OPDs, and the data was processed by Labview measurement software. A homemade transient photovoltage measurement setup was used to measure the frequency of -3dB and transient photoresponse. LED (Thorlabs) with the wavelength of 780 nm and flux density of 1 mW cm^{-2} modulated by the function generator Textronix AFG3102C was used as the light source to illuminate the OPDs. The signal from the OPDs was then collected by a low noise current preamplifier Ametex model 5182 and recorded by oscilloscope Teledyne LeCroy WaveRunner 625 Zi. Impedance spectroscopy was carried out by Solarton Material Lab XM with the frequency of ac signal in the range of 1–10^6 Hz. UV–vis spectrophotometer

(Jasco, V-770) was used in transmittance measurement under ambient condition. The surface morphology was measured by an atomic force microscope (Bruker, INNOVA) with the non-contact mode and the silicon tip (FESPA-V2). For the thermal shock testing, the transparent devices were put on the hotplate at 100 °C with different aging times.

3. Result and discussion

Photocurrent density versus applied voltages characteristics of the OPDs are presented in Fig. 2. All devices show current-gain in the order of 10^6 under the reverse bias of −2 V. However, transparent OPDs offer slightly higher current-gain owing to their lower dark current density (see Table 1). The transparent OPDs show relatively lower dark current density than the reference OPDs in the reversed bias regime (see Fig. 2 (b)). As listed in Table 1, the reference OPDs has the average dark current density of 4.13 nA cm^{-2} under the reversed bias of −2 V. In contrast, the transparent OPDs have a lower average dark current density of 0.36, 0.18, and 0.22 nA cm^{-2} with ClAlPc:C_{60} at the ratio of 1:2, 1:4, and 1:6 respectively. To explain these results, we must consider the origin of the dark current in the OPDs, i.e., the thermal generation process in the photoactive layer [18,33], and the charge injection from metal contacts to organic semiconductor [34–36]. The lower dark current density of transparent OPDs can be attributed to the smoother surface morphology of metal alloy Cu:Ag electrode (RMS = 1.48 nm) compared to Ag electrode (RMS = 3.17 nm) as shown in Fig. S1, which corresponds to a less number of metal-semiconductor interface traps and less charge injection/extraction at the interface [37]. Consequently, the transparent OPDs achieve a lower dark current density [33]. Note that the transparent metal alloy Cu:Ag shows sheet resistance of 16.23 ± 0.31 Ω sq^{-1} while Ag has a significantly lower sheet resistance of 0.28 ± 0.01 Ω sq^{-1}. Ultra-thin and transparent Cu:Ag has a similar conduction property with the ITO (15 Ω sq^{-1}). Moreover, the amount of Ag atom in the thin Cu:Ag electrode is less than the thick Ag electrode, which suggests a fewer organic/metal interface that resulting a lower dark current density in the transparent OPDs [38].

Table 1
The characteristics of OPD devices with various active layer blending ratios.

Device	J_d [nA cm^{-2}][a)]	EQE [%][b)]	R [A W^{-1}][c)]	D* [Jones][d)]	Current-gain [a.u.][e)]
Ref	4.13 ± 0.36	39.4 ± 0.71	0.23 ± 0.004	1.94 × 10^{12}	1.77 × 10^6
1:2	0.36 ± 0.05	29.5 ± 0.36	0.17 ± 0.002	4.12 × 10^{12}	6.16 × 10^6
1:4	0.18 ± 0.02	28.0 ± 0.52	0.17 ± 0.003	3.22 × 10^{12}	6.58 × 10^6
1:6	0.22 ± 0.01	24.9 ± 0.54	0.15 ± 0.003	2.51 × 10^{11}	6.82 × 10^6

a) The values are measured at a reverse bias voltage of −2 V.
b) The value of the spectral responses was measured under reverse bias of −2 V and wavelength 730 nm.
c) The value of the spectral responses was measured under reverse bias of −2 V and wavelength 730 nm.
d) The values are derived from eq. (3), where A = 0.04 cm^2 and normalized bandwidth f = 1 Hz.
e) The current-gain was calculated by J_{photo}/J_{dark} under the applied bias of −2 V.

Fig. 2 (b) shows that a minimum value of dark current density with the positive voltage sweep is observed at around −0.5 V rather than at 0 V. In contrast, when the negative voltage sweep is applied on the same device, the minimum value of dark current density is shifted to 0 V (see Fig. S2). This phenomenon i.e. the shifting of the minimum value is probably caused by the trapped charges in BPhen [39]. This means that the buffer layer of BPhen is crucial to determine the trapping center in our OPD system. For example, Fig. S3 shows that dark current density (transparent OPDs with 1:2 ratio of ClAlPc:C_{60}) is significantly changed after the thermal shock. Furthermore, we replaced BPhen with 1,3,5-Tris

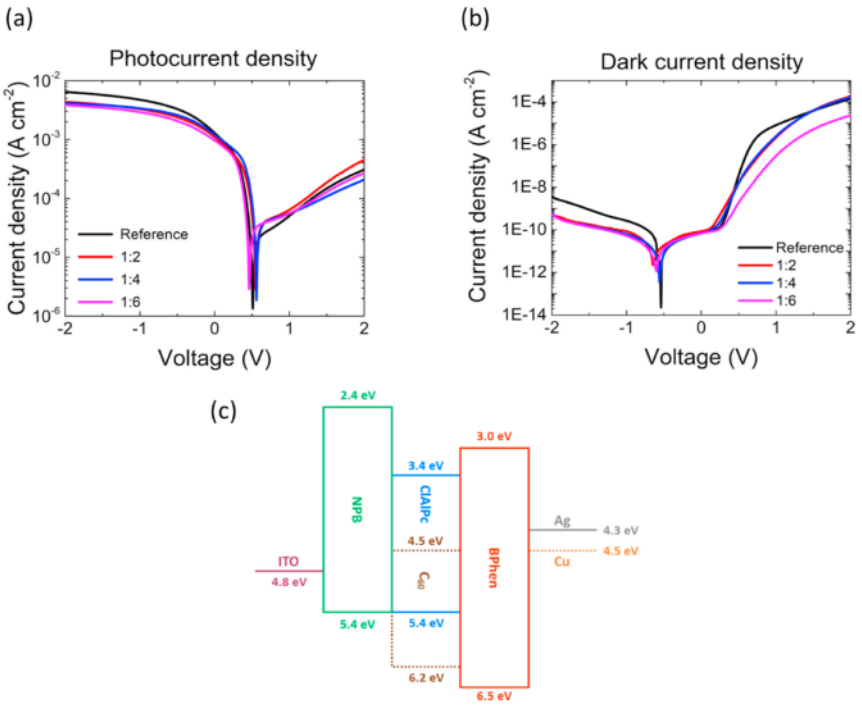

Fig. 2. (a) Photocurrent density-voltage and (b) dark current density-voltage characteristics of the OPDs based on ClAlPc:C_{60} active layer at different mixing ratios. (c) Energy level diagram of the materials following the device structure.

(3-pyridyl-3-phenyl)benzene (TmPyPB) to improve the thermal stability of the transparent OPDs. TmPyPB-based transparent OPDs show a good thermal stability even after 4 h of thermal shock (100 °C). But, we observe that dark current density of TmPyPB-based devices is 10^{-7} A cm^{-2}, which is significantly higher than that of BPhen-based devices. We believe that the trade-off between thermal stability and low dark current density could be resolved in future work by designing a proper blocking material that can achieve both requirements.

The EQE spectra of the OPDs for both bottom and top sides are shown in Fig. 3 (a) and (b). The EQE of the reference OPDs with bottom side illumination (see Fig. 3 (a)) shows a higher value than that of the transparent OPDs. The EQE peaks for the reference OPDs reach 51% and 41% at the wavelength of 375 and 730 nm, respectively. While the transparent OPDs with ClAlPc:C_{60} at the ratio of 1:2, 1:4, and 1:6 can reach 32%, 45%, and 46% at the wavelength of 345 nm; 24%, 27%, and 30% at the wavelength of 730 nm, respectively. The higher EQE values of the reference OPDs are due to a better light trapping capability compared to the transparent OPDs, i.e. Ag electrode serves as a mirror reflecting the incident light [40]. Note that the EQE of transparent OPDs (1:2 ClAlPc:C_{60} ratio) slightly decreases after the thermal shock (see Fig. S4). Fig. 3 (c) and (d) show that the AVT value of transparent OPDs approaches to 77%, while the AVT of photoactive layers (ClAlPc:C_{60}) is higher with the value > 81% (see Fig. S5). The AVT is calculated with the following equation [20]:

$$AVT = \frac{\int_{380nm}^{780nm} T(\lambda)P(\lambda)S(\lambda)d(\lambda)}{\int_{380nm}^{780nm} P(\lambda)S(\lambda)d(\lambda)} \quad (1)$$

where T(λ) is the transmission spectrum, P(λ) is the luminous-efficacy of the human eye, and S(λ) is the incident light correction factor. Interestingly, different ratio of ClAlPc:C_{60} in the active layer of transparent OPDs strongly influences the peak values of the corresponding EQE spectrum. The peak in the UV spectrum increases with the ratio of C_{60}, i.e. the peak in the NIR spectrum decrease accordingly. This is to note that the UV spectrum increases due to the UV absorption characteristic of C_{60} which has a higher ratio in the bulk-heterojunction. In contrast, the NIR spectrum decreases due to the lower ratio of ClAlPc (NIR absorption characteristic). The EQE spectrum shows a similar trend for all transparent OPDs under the top side illumination (Fig. 3 (b)). However, we observed that the device performance under bottom illumination is much better than that under top illumination. Such phenomena can be attributed to the higher transmittance of ITO than Cu:Ag/WO_3 [7,41]. Another parameter that can be derived from the EQE spectrum is responsivity. The responsivity equation can be expressed as:

$$R(\lambda) = EQE\frac{\lambda q}{hc} \quad (2)$$

where R is the responsivity (A W^{-1}), λ (nm) is the wavelength, q (1.602 × 10^{-19} C) is the electron charge, h (J s) is the Planck constant, and c (2.998 × 10^{8} m s^{-1}) is the speed of light. Under bottom side illumination, the reference OPDs show maximum responsivity of 0.24 AW^{-1}, while the maximum responsivity of transparent OPDs is 0.17 AW^{-1} (see Fig. S6 (a)). Furthermore, the responsivity of transparent OPDs under top side illumination is slightly lower than bottom side illumination which exhibit the maximum value of 0.1 AW^{-1} (see Fig. S6 (b)).

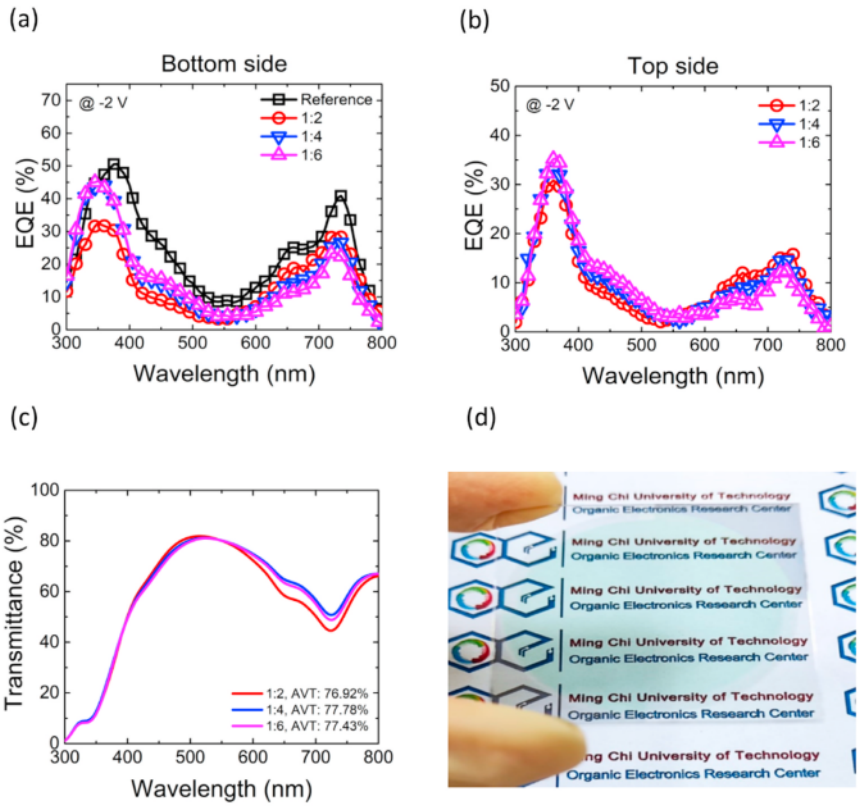

Fig. 3. EQE vs. wavelength for incident light from the (a) bottom and (b) top sides. Note that the device was measured under the voltage of −2 V. (c) The transmission spectra of proposed transparent OPDs. (d) The photograph demonstrates the transparency of a whole structure of transparent OPDs with ClAlPc:C_{60} mixed at 1:2.

A crucial parameter to evaluate the performance of an OPD is its specific detectivity, i.e. OPD's ability to detect the weakest possible signal [10]. The level of specific detectivity is defined as the signal to noise ratio of EQE to dark current noise, which could be evaluated with the following equation [42]:

$$D^* = R\frac{\sqrt{Af}}{i_{noise}} \quad (3)$$

where D* (Jones) is the detectivity, R is the responsivity (A W^{-1}), A (cm^2) is the device's active area, f (Hz) is detection bandwidth, and i_{noise} (A) is noise current in dark condition. Among the parameters defining the equation of specific detectivity, i_{noise} is usually simplified by only considering shot noise, which could overestimate the detectivity value [42,43]. To avoid this case, all current noise components have to be calculated, including shot noise, thermal noise, and 1/f noise. 1/f is called flicker noise which is significant in the low frequency [44], it is negligible for frequency beyond 100 Hz [42]; whereas shot noise and thermal noise (Johnson noise) are the white noise [34]. To get a white noise value, shot noise and thermal noise should be involved in calculating an accurate detectivity value, especially if these noises are in the same order of magnitude [42,45]. The value of shot noise is determined by the dark current, while thermal noise is influenced by the intrinsic value of shunt resistance (R_{SH}) [42]. Both noises could be expressed as the following equations [45,46]:

$$I_{shotnoise} = \sqrt{2qI_{dark}B} \quad (4)$$

$$I_{thermalnoise} = \sqrt{\frac{4kTB}{R_{SH}}} \quad (5)$$

$$I_{noise} = \sqrt{(I_{shotnoise})^2 + (I_{thermalnoise})^2} \quad (6)$$

where q (C) is the electron charge, I_{dark} (A) is the dark current, B (1 Hz) is the normalized bandwidth, k (1.38×10^{-23} J K^{-1}) is the Boltzmann constant, T (K) is the temperature, and R_{SH} (Ω) is the shunt resistance of the OPDs. The R_{SH} value is estimated from the linear fitting of the dark current-voltage plot as shown in Fig. S7. R_{SH} vs voltage is plotted in Fig. S8, where the differential resistance is taken from 0 to 0.2 V; the average value of R_{SH} was determined by the linear fitting method [44]. A better method to get the white noise value is by directly measuring the noise current, which contains all noises simultaneously [42,45]. Based on the current noise calculation as shown in Table 2, shot noise is one order of magnitude higher than thermal noise, in contrast with the result from Lee et al. and Wu et al. that thermal noise dominated noise current [10,42]. In this work, a standard method of calculation which consider only shot noise as noise current (eq. (3)) for detectivity estimation could be used. Furthermore, measured values and calculated values of noise current are close to each other (see Table 2). For better accuracy, the detectivity in this work were calculated from the measurement-based noise current. The measurement-based noise current is calculated with the following equation [47]:

$$I_{noise} = \sqrt{\int_{100Hz}^{1000Hz} [f(\upsilon)]^2 d\upsilon} \quad (7)$$

where υ is the frequency (Hz) and $f(\upsilon)$ is the spectral noise density (A $Hz^{-1/2}$) in Fig. S9. In the applied bias of −2 V and wavelength of 780 nm, detectivity of the reference OPDs is 1.94×10^{12} Jones, while the transparent OPDs with ClAlPc:C_{60} at the ratio of 1:2, 1:4, and 1:6 are 4.12×10^{12}, 3.22×10^{12}, and 2.51×10^{12} Jones, respectively (see Fig. 4). The lower dark current of transparent OPDs is responsible for a higher detectivity value due to the inverse proportion of dark current in the estimation of detectivity. Sub-nA cm^{-2} dark current density of transparent OPDs compensates the lower responsivity values, resulting a higher detectivity value compared to the reference OPDs (nA cm^{-2} dark current density level).

To evaluate the response behavior of OPDs, we measured the LDR with respect to the change in optical illumination power. The optical power versus photocurrent plot could demonstrate OPD's linear response. The linear fitting of the plot to evaluate LDR can be expressed as the following equation [10,45,48,49]:

$$LDR = 20\log\left(\frac{J_{max}}{J_{min}}\right) \quad (8)$$

where LDR is the linear dynamic range (dB), J_{max} (A cm^{-2}) is the maximum photocurrent density, and J_{min} (A cm^{-2}) is the minimum detectable photocurrent density along the linear trajectory. The reference OPDs achieved the LDR of 104.99 dB, while the transparent OPDs with ClAlPc:C_{60} at the ratio of 1:2, 1:4, and 1:6 achieved the LDR of 111.04, 93.46, and 100.43 dB, respectively (see Fig. 5). The LDR results show a linear characteristic in the log-log plot of the photocurrent vs illumination power with the slope of 0.95, 1.01, 0.98, and 1.02 for the reference OPDs and the transparent OPDs with the active layer ratio of 1:2, 1:4, and 1:6, respectively. Furthermore, the dark current started to dominate the measured photocurrent in the lowest illumination power density (see Fig. 5). As can be seen in Table S1, the generated

Table 2
The summary of noise currents by the following eq. (4), eq. (5), and eq. (6).

Device	R_{SH} [GΩ][a]	I_{dark} [pA][b]	I_{shot} [fA][c]	$I_{thermal}$ [fA][d]	I_{noise} [fA][e]	$I_{noise,measured}$ [fA][f]
Ref	156	165	7.27	0.32	7.28	7.765
1:2	113	14.4	2.15	0.38	2.18	2.82
1:4	61	7.2	1.52	0.52	1.61	2.88
1:6	212	8.8	1.68	0.28	1.70	2.87

[a] The values are calculated from the linear fitting of dark current-voltage in Fig. S7.
[b] The values correspond to the dark current density of the device with the area of 0.04 cm^2 and applied bias −2 V.
[c] The values are derived from eq. (4), where $q = 1.602 \times 10^{-19}$ C and B = 1 Hz (normalized bandwidth).
[d] The values are derived from eq. (5), where $k = 1.38 \times 10^{-23}$ J K^{-1}, T = 298 K, and B = 1 Hz.
[e] The values are derived from eq. (6).
[f] The values are based on the RMS value of noise spectral density as shown in Fig. S9.

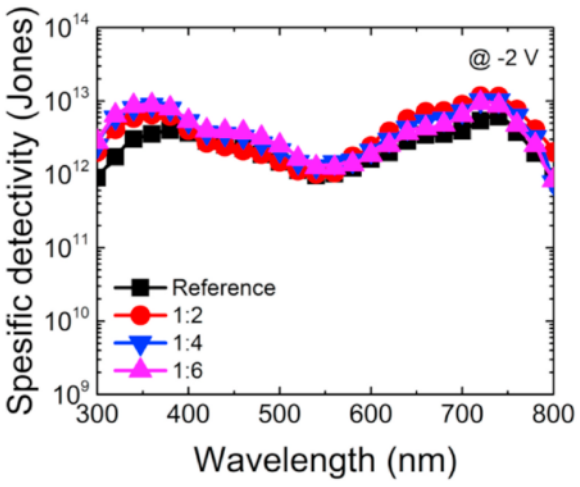

Fig. 4. Specific detectivity of the OPDs under the voltage of −2 V.

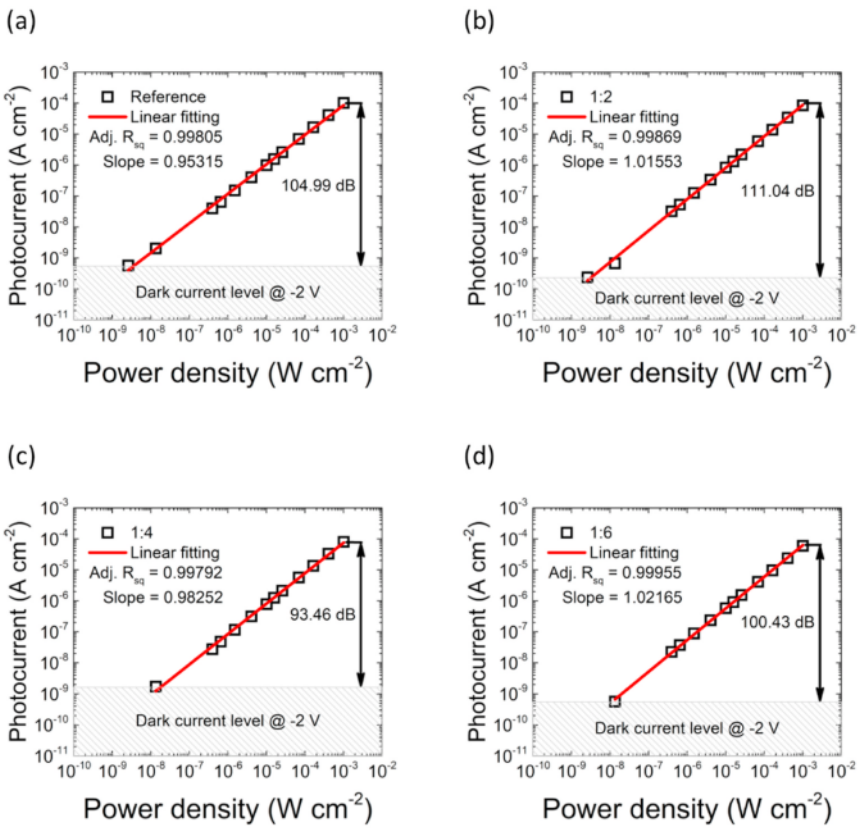

Fig. 5. The LDR measurements of OPD devices at a bias of −2 V under 780 nm radiant flux from 1 mW cm^{-2} to 1 nW cm^{-2} for (a) the reference OPDs, and the transparent OPDs with the active layer ratios of (b) 1:2, (c) 1:4, and (d) 1:6. The slope is the gradient of linear fitting, R_{sq} is the mean square deviation from the linear fitting.

photocurrent is only a fraction of the measured photocurrent, which indicates dark current dominates measured photocurrent in the lowest illumination power.

Another critical parameter that determines OPD's performance is its frequency response. This parameter is evaluated based on the cut off frequency (known as f_{-3dB}), which corresponds to a -3dB signal attenuation or 50% of the steady-state signal power; mathematically, it is a function of slower carrier's transit time and RC-time of the OPDs and given by Refs. [45,48,50]:

$$\frac{1}{f_{-3dB}^2} = \left(\frac{2\pi t}{3.5}\right)^2 + (2\pi R_t C)^2 \tag{9}$$

where f_{-3dB} is the cut-off frequency (Hz), t (s) is the carrier transit time, R_t (Ω) is the total series resistance, and C (F) is the capacitance of photodetector. The RC-time constant would dominate the f_{-3dB} as the device's area scaled up due to the size effect [51]. Consequently, only the limited bandwidth of RC-time significantly influences the cut off frequency. Hence, the f_{-3dB} can be written in the following form [45]:

$$f_{-3dB} = \frac{1}{2\pi R_t C} \tag{10}$$

The f_{-3dB} measurement shows that the reference OPDs offer the highest limited bandwidth, which is slightly higher than that of the transparent OPDs with ClAlPc:C_{60} at 1:2, 1:4, and 1:6 ratios. The values for the transparent OPDs are 763.15, 639.54, 539.84, and 493.04 kHz, respectively (see Fig. 6 (a)). The f_{-3dB} values decrease with the increase of the C_{60} ratio for transparent OPDs due to the increase in resistance (Table S2). Based on eq. (10), the resistance increment reduces the bandwidth of -3dB since it is inversely proportional to f_{-3dB}. As a complementary measurement, the transient photovoltage study is proposed to investigate the response time of the OPDs when a modulated optical signal is illuminated on it by measuring the rise and fall time of the response [49]. Rise time is the interval of time that is needed by photovoltage to rise from 10% to 90% of its maximum value, whereas its fall from 90% to 10% is identified as fall time [52]. As displayed in Fig. 6 (b), (c), and (d), the transparent OPDs with ClAlPc:C_{60} at the ratio of 1:2 demonstrate the response time faster compared to the other ratios (see Table S2 for the details). These results can be attributed to the early dissociation of excitons in ClAlPc:C_{60} with 1:2 ratio compared to other ratios [53].

4. Conclusions

In this work, an efficient and transparent OPD with high AVT and fast-photoresponse was achieved. The optimized device exceeded the reference OPDs in several aspects, such as dark current density and detectivity. It has been shown that the optimized transparent OPDs with ClAlPc:C_{60} at 1:2 ratio offers a average dark current density of 0.36 nA cm^{-2} and detectivity of 4.12×10^{12} Jones, while the reference OPDs have an average dark current density of 4.13 nA cm^{-2} and detectivity of 1.94×10^{12} Jones. The lower dark current density possessed by the transparent OPDs originates from the utilization of Cu:Ag/WO_3 as the transparent metal electrode in the device structure. Moreover, the

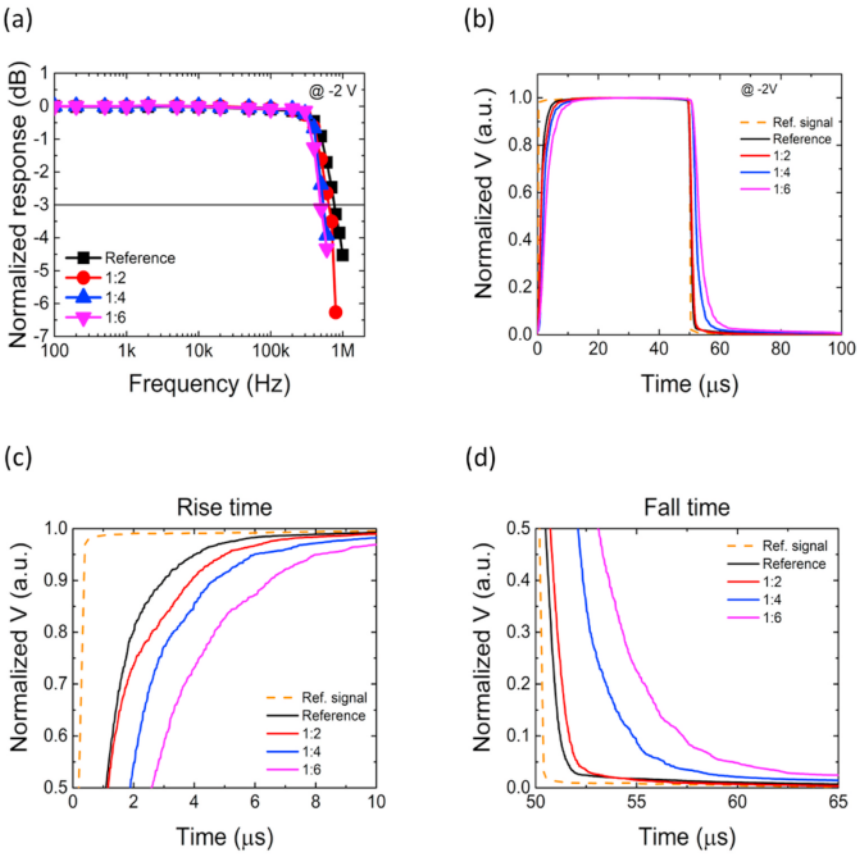

Fig. 6. The response curve of the OPDs under bias −2 V and 1 mW cm^{-2} 780 nm illumination with modulated frequency. (a) Normalized frequency response curve. (b) Normalized transient photovoltage curve. (c) Rise time and (d) fall time from the normalized transient photovoltage measurements.

optimized transparent OPDs showed the AVT of 76.92% and the rise/fall time <5 μs, which could be potentially applied in the home security system based on invisible light detection.

CRediT authorship contribution statement

Marvin Yonathan Hadiyanto: Conceptualization, Investigation, Writing – Original Draft. **Richie Estrada:** Visualization, Writing – Review & Editing. **Chih-Chien Lee:** Formal analysis, Methodology. **Sajal Biring:** Validation, Writing – Review & Editing. **Abdul Khalik Akbar:** Investigation, Software. **Chien-Yi Li:** Resources. **Chun-Jen Shih:** Data curation, Validation. **Ya-Ze Li:** Supervision. **Shun-Wei Liu:** Conceptualization, Methodology, Supervision, Project administration, Funding acquisition, Writing – Review & Editing.

Declaration of competing interest

The authors declare that they have no known competing financial interests or personal relationships that could have appeared to influence the work reported in this paper.

Acknowledgements

The authors acknowledge financial support from the Ministry of Science and Technology (Grant Nos. MOST 109-2221-E-011-156, 110-2221-E-131-019, and 109-2223-E-131-001-MY3. The corresponding author (S.-W. Liu) is grateful to Mr. H.-H. Wu, Syskey Technology Co., Ltd (Taiwan), for his assistance in designing the fabrication system. Also, the authors thank Maya Angela for helping to prepare the picture for graphical abstract.

Appendix A. Supplementary data

Supplementary data to this article can be found online at https://doi.org/10.1016/j.orgel.2021.106356.

References

[1] T.N. Ng, W.S. Wong, R.A. Lujan, R.A. Street, Characterization of charge collection in photodiodes under mechanical strain: comparison between organic bulk heterojunction and amorphous silicon, Adv. Mater. 21 (2009) 1855–1859, https://doi.org/10.1002/adma.200803046.
[2] R.D. Jansen-van Vuuren, A. Armin, A.K. Pandey, P.L. Burn, P. Meredith, Organic photodiodes: the future of full color detection and image sensing, Adv. Mater. 28 (2016) 4766–4802, https://doi.org/10.1002/adma.201505405.
[3] K.H. An, B. O'Connor, K.P. Pipe, M. Shtein, Organic photodetector with spectral response tunable across the visible spectrum by means of internal optical microcavity, Org. Electron. 10 (2009) 1152–1157, https://doi.org/10.1016/j.orgel.2009.06.003.
[4] H. Tanaka, T. Yasuda, K. Fujita, T. Tsutsui, Transparent image sensors using an organic multilayer photodiode, Adv. Mater. 18 (2006) 2230–2233, https://doi.org/10.1002/adma.200600163.
[5] M.R. Esopi, Q. Yu, Plasmonic aluminum nanohole arrays as transparent conducting electrodes for organic ultraviolet photodetectors with bias-dependent photoresponse, ACS Appl. Nano Mater. 2 (2019) 4942–4953, https://doi.org/10.1021/acsanm.9b00902.
[6] X. Wang, H. Wang, D. Zhou, H. Jin, J. Yu, Semitransparent indium-tin-oxide-free non-fullerene organic photodetectors with double-side ultraviolet selective

responses, Mater. Lett. 230 (2018) 289–292, https://doi.org/10.1016/j.matlet.2018.07.121.
[7] D. Zhao, M. Wu, R. Qin, J. Yu, Low dark-current and high-photodetectivity transparent organic ultraviolet photodetector by using polymer-modified ZnO as the electron transfer layer, Opt. Lett. 43 (2018) 3212, https://doi.org/10.1364/ol.43.003212.
[8] Z. Liu, K. Parvez, R. Li, R. Dong, X. Feng, K. Müllen, Transparent conductive electrodes from graphene/PEDOT:PSS hybrid inks for ultrathin organic photodetectors, Adv. Mater. 27 (2015) 669–675, https://doi.org/10.1002/adma.201403826.
[9] D.H. Kim, K.S. Kim, H.S. Shim, C.K. Moon, Y.W. Jin, J.J. Kim, A high performance semitransparent organic photodetector with green color selectivity, Appl. Phys. Lett. 105 (2014) 213301, https://doi.org/10.1063/1.4902871.
[10] C.C. Lee, R. Estrada, Y.Z. Li, S. Biring, N.R. Al Amin, M.Z. Li, S.W. Liu, K.T. Wong, Vacuum-processed small molecule organic photodetectors with low dark current density and strong response to near-infrared wavelength, Adv. Opt. Mater. 8 (2020) 1–10, https://doi.org/10.1002/adom.202000519.
[11] B. Verreet, R. Müller, B.P. Rand, K. Vasseur, P. Heremans, Structural templating of chloro-aluminum phthalocyanine layers for planar and bulk heterojunction organic solar cells, Org. Electron. 12 (2011) 2131–2139, https://doi.org/10.1016/j.orgel.2011.08.031.
[12] M.Z. Li, C.C. Lee, S. Biring, I.S. Hsu, D. Luo, R. Estrada, Y.S. Wu, C.C. Yang, S. W. Liu, Vacuum-deposited transparent organic photovoltaics for efficiently harvesting selective ultraviolet and near-infrared solar Energy, Sol. RRL. (2020) 1–11, https://doi.org/10.1002/solr.202000564, 2000564.
[13] B. Verreet, R. Müller, B.P. Rand, K. Vasseur, P. Heremans, Structural templating of chloro-aluminum phthalocyanine layers for planar and bulk heterojunction organic solar cells, Org. Electron. 12 (2011) 2131–2139, https://doi.org/10.1016/j.orgel.2011.08.031.
[14] Z. Wei, Y. Liu, S. Xiao, X. Li, N. Zhong, H. Liu, F. Wang, R. Liang, Angular and wavelength simultaneous selection in transparent OPVs based on near-infrared Bragg reflector and antireflection coating, IEEE Photonics J 9 (2017) 7800908, https://doi.org/10.1109/JPHOT.2016.2644961.
[15] Q. Jiang, Y. Xing, Improved performance of small molecule organic solar cells by incorporation of a glancing angle deposited donor layer, Sci. Rep. 10 (2020) 1–10, https://doi.org/10.1038/s41598-020-62769-3.
[16] J.W. Seo, S.H. Lee, J.Y. Lee, Enhancing quantum efficiency of parallel-like bulk heterojunction solar cells, Appl. Phys. Lett. 103 (2013) 123301, https://doi.org/10.1063/1.4821441.
[17] K. Harada, T. Edura, C. Adachi, Nanocrystal growth and improved performance of small molecule bulk heterojunction solar cells composed of a blend of chloroaluminum phthalocyanine and C70, APEX 3 (2010) 1–4, https://doi.org/10.1143/APEX.3.121602.
[18] H. Shekhar, O. Solomeshch, D. Liraz, N. Tessler, Low dark leakage current in organic planar heterojunction photodiodes, Appl. Phys. Lett. 111 (2017) 223301, https://doi.org/10.1063/1.4996826.
[19] C.J. Shih, Y.Z. Li, M.Z. Li, S. Biring, B.C. Huang, C.W. Liu, T.H. Yeh, D. Luo, J. H. Lee, Y.H. Huang, K.T. Wong, S.W. Liu, Transparent organic upconversion device targeting high- grade infrared visual image, Nano Energy 86 (2021) 106043, https://doi.org/10.1016/j.nanoen.2021.106043.
[20] Y.S. Lau, Z. Lan, L. Cai, F. Zhu, High-performance solution-processed large-area transparent self-powered organic near-infrared photodetectors, Mater. Today Energy. 21 (2021) 100708, https://doi.org/10.1016/j.mtener.2021.100708.
[21] S.W. Liu, T.H. Su, P.C. Chang, T.H. Yeh, Y.Z. Li, L.J. Huang, Y.H. Chen, C.F. Lin, ITO-free, efficient, and inverted phosphorescent organic light-emitting diodes using a WO3/Ag/WO3 multilayer electrode, Org. Electron. 31 (2016) 240–246, https://doi.org/10.1016/j.orgel.2016.01.035.
[22] K. Hong, K. Kim, S. Kim, I. Lee, H. Cho, S. Yoo, H.W. Choi, N.Y. Lee, Y.H. Tak, J. L. Lee, Optical properties of WO3/Ag/WO3 multilayer as transparent cathode in top-emitting organic light emitting diodes, J. Phys. Chem. C 115 (2011) 3453–3459, https://doi.org/10.1021/jp109943b.
[23] T.H. Yeh, C.C. Lee, C.J. Shih, G. Kumar, S. Biring, S.W. Liu, Vacuum-deposited MoO3/Ag/WO3 multilayered electrode for highly efficient transparent and inverted organic light-emitting diodes, Org. Electron. 59 (2018) 266–271, https://doi.org/10.1016/j.orgel.2018.05.014.
[24] G.H. Jung, K. Hong, W.J. Dong, S. Kim, J.L. Lee, BCP/Ag/MoO 3 transparent cathodes for organic photovoltaics, Adv. Energy Mater. 1 (2011) 1023–1028, https://doi.org/10.1002/aenm.201100411.
[25] S.W. Liu, T.H. Su, Y.Z. Li, Ultra-thin and graded sliver electrodes for use in transparent pentacene field-effect transistors, Org. Electron. 15 (2014) 1990–1997, https://doi.org/10.1016/j.orgel.2014.05.037.
[26] F. Wang, Z. Chen, L. Xiao, B. Qu, Q. Gong, Papery solar cells based on dielectric/metal hybrid transparent cathode, Sol. Energy Mater. Sol. Cells 94 (2010) 1270–1274, https://doi.org/10.1016/j.solmat.2010.03.023.
[27] L.H. Xu, Q.D. Ou, Y.Q. Li, Y.B. Zhang, X.D. Zhao, H.Y. Xiang, J. De Chen, L. Zhou, S.T. Lee, J.X. Tang, Microcavity-free broadband light outcoupling enhancement in flexible organic light-emitting diodes with nanostructured transparent metal-dielectric composite electrodes, ACS Nano 10 (2016) 1625–1632, https://doi.org/10.1021/acsnano.5b07302.
[28] H. Zhang, S. Jenatsch, J. De Jonghe, F. Nuësch, R. Steim, A.C. Véron, R. Hany, Transparent organic photodetector using a near-infrared absorbing cyanine dye, Sci. Rep. 5 (2015) 1–6, https://doi.org/10.1038/srep09439.
[29] H.S. Kim, K.R. Chauhan, J. Kim, E.H. Choi, Flexible vanadium oxide film for broadband transparent photodetector, Appl. Phys. Lett. 110 (2017) 101907, https://doi.org/10.1063/1.4977426.
[30] K.B. Ko, B.D. Ryu, M. Han, C.H. Hong, D.A. Dinh, T.V. Cuong, Multidimensional graphene and ZnO-based heterostructure for flexible transparent ultraviolet photodetector, Appl. Surf. Sci. 481 (2019) 524–530, https://doi.org/10.1016/j.apsusc.2019.03.163.
[31] D.B. Patel, K.R. Chauhan, S.H. Park, J. Kim, High-performing transparent photodetectors based on Schottky contacts, Mater. Sci. Semicond. Process. 64 (2017) 137–142, https://doi.org/10.1016/j.mssp.2017.03.024.
[32] Y. Li, Y. Li, J. Chen, Z. Sun, Z. Li, X. Han, P. Li, X. Lin, R. Liu, Y. Ma, W. Huang, Full-solution processed all-nanowire flexible and transparent ultraviolet photodetectors, J. Mater. Chem. C. 6 (2018) 11666–11672, https://doi.org/10.1039/c8tc04044c.
[33] A.H. Fallahpour, S. Kienitz, P. Lugli, Origin of dark current and detailed description of organic photodiode operation under different illumination intensities, IEEE Trans. Electron. Dev. 64 (2017) 2649–2654, https://doi.org/10.1109/TED.2017.2696478.
[34] M. Kielar, O. Dhez, G. Pecastaings, A. Curutchet, L. Hirsch, Long-term stable organic photodetectors with ultra low dark currents for high detectivity applications, Sci. Rep. 6 (2016) 1–11, https://doi.org/10.1038/srep39201.
[35] X. Zhou, D. Yang, D. Ma, Extremely low dark current, high responsivity, all-polymer photodetectors with spectral response from 300 nm to 1000 nm, Adv. Opt. Mater. 3 (2015) 1570–1576, https://doi.org/10.1002/adom.201500224.
[36] G.H. Gelinck, A. Kumar, D. Moet, J.L.P.J. Van Der Steen, A.J.J.M. Van Breemen, S. Shanmugam, A. Langen, J. Gilot, P. Groen, R. Andriessen, M. Simon, W. Ruetten, A.U. Douglas, R. Raaijmakers, P.E. Malinowski, K. Myny, X-ray detector-on-plastic with high sensitivity using low cost, solution-processed organic photodiodes, IEEE Trans. Electron. Dev. 63 (2016) 197–204, https://doi.org/10.1109/TED.2015.2432572.
[37] L. Du, H. Li, L. Yan, J. Zhang, Q. Xin, Q. Wang, A. Song, Effects of substrate and anode metal annealing on InGaZnO Schottky diodes, Appl. Phys. Lett. 110 (2017), 011602, https://doi.org/10.1063/1.4973693.
[38] X. Hao, S. Wang, W. Fu, T. Sakurai, S. Masuda, K. Akimoto, Novel cathode buffer layer of Ag-doped bathocuproine for small molecule organic solar cell with inverted structure, Org. Electron. 15 (2014) 1773–1779, https://doi.org/10.1016/j.orgel.2014.04.030.
[39] D. Splith, S. Müller, H. von Wenckstern, M. Grundmann, Numerical modeling of Schottky Barrier diode characteristics, Phys. Status Solidi Appl. Mater. Sci. 218 (2021), https://doi.org/10.1002/pssa.202100121.
[40] S. Esiner, T. Bus, M.M. Wienk, K. Hermans, R.A.J. Janssen, Quantification and validation of the efficiency enhancement reached by application of a retroreflective light trapping texture on a polymer solar cell, Adv. Energy Mater. 3 (2013) 1013–1017, https://doi.org/10.1002/aenm.201300227.
[41] W.F. Xie, K.C. Lau, C.S. Lee, S.T. Lee, Transparent organic light-emitting devices with LiF/Yb:Ag cathode, Thin Solid Films 515 (2007) 6975–6977, https://doi.org/10.1016/j.tsf.2007.02.008.
[42] Z. Wu, W. Yao, A.E. London, J.D. Azoulay, T.N. Ng, Elucidating the detectivity limits in shortwave infrared organic photodiodes, Adv. Funct. Mater. 28 (2018) 1–9, https://doi.org/10.1002/adfm.201800391.
[43] Y. Fang, J. Huang, Resolving weak light of sub-picowatt per square centimeter by hybrid perovskite photodetectors enabled by noise reduction, Adv. Mater. 27 (2015) 2804–2810, https://doi.org/10.1002/adma.201500099.
[44] R. Dong, Y. Fang, J. Chae, J. Dai, Z. Xiao, Q. Dong, Y. Yuan, A. Centrone, X.C. Zeng, J. Huang, High-gain and low-driving-voltage photodetectors based on organolead triiodide perovskites, Adv. Mater. 27 (2015) 1912–1918, https://doi.org/10.1002/adma.201405116.
[45] A. Armin, M. Hambsch, I.K. Kim, P.L. Burn, P. Meredith, E.B. Namdas, Thick junction broadband organic photodiodes, Laser Photon. Rev. 8 (2014) 924–932, https://doi.org/10.1002/lpor.201400081.
[46] Z. Lan, Y. Lei, W.K.E. Chan, S. Chen, D. Luo, F. Zhu, Near-infrared and visible light dual-mode organic photodetectors, Sci. Adv. 6 (2020) 1–10, https://doi.org/10.1126/sciadv.aaw8065.
[47] N. Strobel, M. Seiberlich, R. Eckstein, U. Lemmer, G. Hernandez-Sosa, Organic photodiodes: printing, coating, benchmarks, and applications, Flex. Print. Electron. 4 (2019) 43001, https://doi.org/10.1088/2058-8585/ab56dd.
[48] F.P. García De Arquer, A. Armin, P. Meredith, E.H. Sargent, Solution-processed semiconductors for next-generation photodetectors, Nat. Rev. Mater. 2 (2017) 1–16, https://doi.org/10.1038/natrevmats.2016.100.
[49] X. Liu, Y. Lin, Y. Liao, J. Wu, Y. Zheng, Recent advances in organic near-infrared photodiodes, J. Mater. Chem. C. 6 (2018) 3499–3513, https://doi.org/10.1039/c7tc05042a.
[50] K. Kato, Ultrawide-B and/high-frequency photodetectors, IEEE Trans. Microw. Theor. Tech. 47 (1999) 1265–1281, https://doi.org/10.1109/22.775466.
[51] C.C. Lee, S. Biring, S.J. Ren, Y.Z. Li, M.Z. Li, N.R. Al Amin, S.W. Liu, Reduction of dark current density in organic ultraviolet photodetector by utilizing an electron blocking layer of TAPC doped with MoO3, Org. Electron. 65 (2019) 150–155, https://doi.org/10.1016/j.orgel.2018.11.016.
[52] T. Morimune, H. Kajii, Y. Ohmori, Photoresponse properties of a high-speed organic photodetector based on copper-phthalocyanine under red light illumination, IEEE Photon. Technol. Lett. 18 (2006) 2662–2664, https://doi.org/10.1109/LPT.2006.887786.
[53] T. Morimune, H. Kajii, Y. Ohmori, Frequency response properties of organic photodetectors as opto-electrical conversion devices, IEEE/OSA J. Disp. Technol. 2 (2006) 170–174, https://doi.org/10.1109/JDT.2006.874505.

Transparent photodetectors with ultra-low dark current and high photoresponse for near-infrared detection

ORIGINALITY REPORT

4%	3%	4%	1%
SIMILARITY INDEX	INTERNET SOURCES	PUBLICATIONS	STUDENT PAPERS

PRIMARY SOURCES

1	pubs.rsc.org Internet Source	1%
2	Junwei Liu, Mengyuan Gao, Juhee Kim, Zhihua Zhou, Dae Sung Chung, Hang Yin, Long Ye. "Challenges and recent advances in photodiodes-based organic photodetectors", Materials Today, 2021 Publication	1%
3	spiral.imperial.ac.uk Internet Source	1%
4	www.researchgate.net Internet Source	1%
5	Dae-Ho Kim, Kyu-Sik Kim, Hyun-Sub Shim, Chang-Ki Moon, Yong Wan Jin, Jang-Joo Kim. "A high performance semitransparent organic photodetector with green color selectivity", Applied Physics Letters, 2014 Publication	1%

6	Il Ku Kim, Bhola N. Pal, Mujeeb Ullah, Paul L. Burn, Shih-Chun Lo, Paul Meredith, Ebinazar B. Namdas. "High-Performance, Solution-Processed Non-polymeric Organic Photodiodes", Advanced Optical Materials, 2015 Publication	1 %

Exclude quotes	Off	Exclude matches	< 1%
Exclude bibliography	On		